# Open Research Online

The Open University's repository of research publications
and other research outputs

# Fluctuation-exchange supplemented quantum Monte Carlo approach to the Hubbard model

## Journal Item

Version: [not recorded]

## oro.open.ac.uk

# A novel FLEX supplemented QMC approach to the Hubbard model

J.P. Hague,[1,2] Mark Jarrell,[1] and T.C.Schulthess[2]

[1]*Department of Physics, University of Cincinnati*
[2]*Computer science and mathematics division, Oak Ridge National Laboratory*
(Dated: May 13, 2009)

This paper introduces a novel ansatz-based technique for solution of the Hubbard model over two length scales. Short range correlations are treated exactly using a dynamical cluster approximation QMC simulation, while longer-length-scale physics requiring larger cluster sizes is incorporated through the introduction of the fluctuation exchange (FLEX) approximation. The properties of the resulting hybrid scheme are examined, and the description of local moment formation is compared to exact results in 1D. The effects of electron-electron coupling and electron doping on the shape of the Fermi-surface are demonstrated in 2D. Causality is examined in both 1D and 2D. We find that the scheme is successful if QMC clusters of $N_C \geq 4$ are used (with sufficiently high temperatures in 1D), however very small QMC clusters of $N_C = 1$ lead to acausal results. [**PUBLISHED AS: Phys. Rev. B 69, 165113 (2004)**]

## I. INTRODUCTION

Despite its transparent meaning and simple form, the Hubbard model is thought to contain much of the fundamental physics of correlated electron systems [1]. Since its inception, the Hubbard model has been successfully applied to the description of the Mott–Hubbard metal-insulator transition, and is thought to contain a minimal description of certain transition metal oxides, such as the high-$T_C$ cuprates and the low-$T_C$ ruthenates. While limiting aspects of the model are easily understood, the exact ground state of the one-band Hubbard model remains unknown for all cases other than the Hubbard chain [2].

Examination of the infinite-dimensional limit of the Hubbard model using dynamical mean-field theory (DMFT) has lead to a greater understanding of intermediate coupling phenomena such as the Mott-Hubbard metal-insulator transition [3]. DMFT maps the full lattice problem onto a single impurity Anderson model, which may be solved using various numerically exact techniques such as quantum Monte-Carlo (QMC) [4] and numerical renormalization group (NRG) [5]. In recent work, the dynamical mean-field theory was extended to study correlated electron systems in 2D, resulting in an approach known as the dynamical cluster approximation (DCA) [6]. DCA is a fully causal method, which systematically restores non-local corrections to the dynamical mean-field theory. In previous work, Jarrell *et al.* computed the phase diagram of the 2D Hubbard model for small clusters of $N_C = 4$ using QMC [7]. Unfortunately, the QMC solution of large clusters is prohibitively expensive in terms of super-computer time, while alternative approaches, such as the perturbation-theory-based FLEX approximation can be used to solve large DCA clusters, but only in certain limits. FLEX is physically intuitive, concentrating on scattering from important mechanisms (spin fluctuation, density fluctuation and particle-particle pairs), and in the past, FLEX has been shown to reproduce long-length-scale physics of the Hubbard model such as the Mermin–Wagner theorem [8].

In this paper we present an ansatz for combining long length scale information from the FLEX approximation with the QMC solution of the Hubbard model. The two techniques are complimentary, since QMC predicts the correct short length scale physics, while FLEX shows appropriate long length-scale behavior. In section II, we introduce the DCA and the ansatz for the self-energy, and provide technical details of the modified self-consistent procedure for the incorporation of two-length-scale physics. We examine issues of causality and applicability in section III. In section IV we examine local moment formation and the momentum dependent occupation $n_{\mathbf{k}}$. Comparisons are made between the hybrid technique introduced here, exact results for the 1D model and the more traditional FLEX technique. We calculate the Fermi surface of the 2D model in section V. Finally, we discuss the applicability and outlook for the new technique in section VI

## II. FORMALISM

The DCA extends the DMFT, which assumes that the self-energy is constant across the Brillouin Zone (BZ), by introducing a limited momentum dependence corresponding to short range spatial fluctuations. This is achieved by breaking up the Brillouin zone into a series of subzones, within which it is assumed that the self-energy is constant. This allows a momentum integrated (or coarse grained) Green function to be defined in an analogous manner to the definition of DMFT:

$$\bar{G}(i\omega_n, \mathbf{K}_i) = \sum_{k \in \text{subzone}} \frac{1}{i\omega_n + \mu - \epsilon_k - \Sigma(i\omega_n, \mathbf{K}_i)} \quad (1)$$

The $\mathbf{K}_i$ are defined as in reference 6 as the mean momentum for a coarse grained cell. Via an inverse Dyson equation, this leads to a "bare" Green function corre-

sponding to the host of a cluster impurity problem,

$$\Sigma(\mathbf{K}, i\omega_n) = \mathcal{G}_0^{-1}(\mathbf{K}, i\omega_n) - \bar{G}^{-1}(\mathbf{K}, i\omega_n). \quad (2)$$

which may be solved with a variety of methods. The approximation has two well defined limiting cases. For cluster sizes of 1, the DCA maps onto the DMFT. For infinite subzones, the formalism is exact. For a finite number of subzones, results are expected to be closer to the behavior of the exact infinite lattice than conventional finite size techniques, since an infinite number of **k**-states is considered. The coarse graining over **k**-states maps the lattice model to be studied (in this case the Hubbard model) onto a periodic cluster in real space.

In order to solve the resulting problem, approximations

are employed. Two common cluster solvers are the FLEX approximation [9], and the QMC method of Hirsch and Fye [10, 11]. In principle, the QMC method gives the exact solution of the cluster, but the numerical cost is high, and only small clusters can be investigated. Details of the QMC and FLEX methods may be found in references 4 and 8 respectively.

In the hybrid technique proposed here, we define clusters of two sizes, one large of size $N'_C$ solved with the FLEX, and one small of size $N_C$ solved with QMC. For the small cluster, coarse grained points are denoted **K**, and for the large cluster, they are denoted as **K**′. In order to couple the self energies from these methods, we define an ansatz [**?** ]:

$$\Sigma^{(N_C)}(\mathbf{K}, i\omega_n) = \Sigma_{\mathrm{QMC}}^{(N_C)}(\mathbf{K}, i\omega_n) - \Sigma_{\mathrm{FLEX}}^{(N_C)}(\mathbf{K}, i\omega_n) + \bar{\Sigma}_{\mathrm{FLEX}}^{(N'_C)}(\mathbf{K}, i\omega_n) \quad (3)$$

$$\Sigma^{(N'_C)}(\mathbf{K}', i\omega_n) = \bar{\Sigma}_{\mathrm{QMC}}^{(N_C)}(\mathbf{K}', i\omega_n) - \bar{\Sigma}_{\mathrm{FLEX}}^{(N_C)}(\mathbf{K}', i\omega_n) + \Sigma_{\mathrm{FLEX}}^{(N'_C)}(\mathbf{K}', i\omega_n) \quad (4)$$

The superscripts indicate the size of the cluster. Bars over the self energy indicate that a secondary coarse graining of the lattice self energy (linear interpolated self energy) from the other cluster size has been performed, i.e.

$$\bar{\Sigma}(\mathbf{K}', i\omega_n) = \sum_{k \in K'} \Sigma(\mathbf{k}, i\omega_n) \quad (5)$$

where $\Sigma(\mathbf{k}, i\omega_n)$ is the linear interpolation (lattice self-energy) of the small cluster (an equivalent expression exists to coarse grain from the large to the small cluster).

The physical content of the ansatz can be clarified by examining the diagrammatic expansion in figure 1. Since the QMC self energy is non-perturbative, it contains complete contributions from all orders in $U$ for a cluster of size $N_C$ (1st term). The second term removes all FLEX contributions for cluster size $N_C$. These are then replaced with the FLEX contributions for the larger cluster size $N'_C$. This approach is reasonable if the set of FLEX diagrams have a stronger momentum dependence than the remaining diagrams. The complete FLEX with particle-particle scattering obeys the Mermin–Wagner theorem in 2D, indicating a significant momentum dependence which partially justifies this assumption.

As there are two length scales represented in the ansatz, two coarse grainings and cluster exclusions are performed consecutively (one for each length scale). The cluster excluded Green function for the small cluster is then used as input to the QMC, and the coarse grained Green functions are used as input to the FLEX. This leads to an iterative procedure which is demonstrated in figure 2. There are some additional methods that can be

employed to aid convergence. The FLEX self-energy is strongly damped between iterations to avoid the FLEX instability, and many FLEX iterations $\sim 100$ are carried out for each QMC step (the ansatz is recomputed on each sub-iteration of the FLEX). The QMC step is also damped to a lesser degree.

## III.   RANGE OF APPLICABILITY

Causality is essential for any predictive theory. Causality violations in single-particle quantities can lead to negative parts of the single-particle spectrum and density of states and violations of sum rules. Causality violations in two-particle quantities can lead to erroneous predictions for phase transitions. This section examines how causality problems can arise, the expected regions of applicability for the new approximation, and tactics that may be employed to avoid numerical instabilities. Causality is reflected in the analytic properties of the self energy and Green functions. For example, the retarded self energy $\Sigma(\mathbf{k}, \omega)$ is analytic in the upper half of the complex frequency plane and $-\frac{1}{\pi}\mathrm{Im}\Sigma(\mathbf{k}, \omega) > 0$. Since there is a subtraction in the ansatz for the self-energy, causality problems might be anticipated, since the imaginary part of the real-frequency self-energy can become positive. Here, we search for causality violations in the Matsubara self energy. It is related to $\Sigma(\mathbf{k}, \omega)$ through

$$\Sigma(\mathbf{k}, i\omega_n) = \int d\omega \frac{-\frac{1}{\pi}\mathrm{Im}\Sigma(\mathbf{k}, \omega)}{i\omega_n - \omega} \quad (6)$$
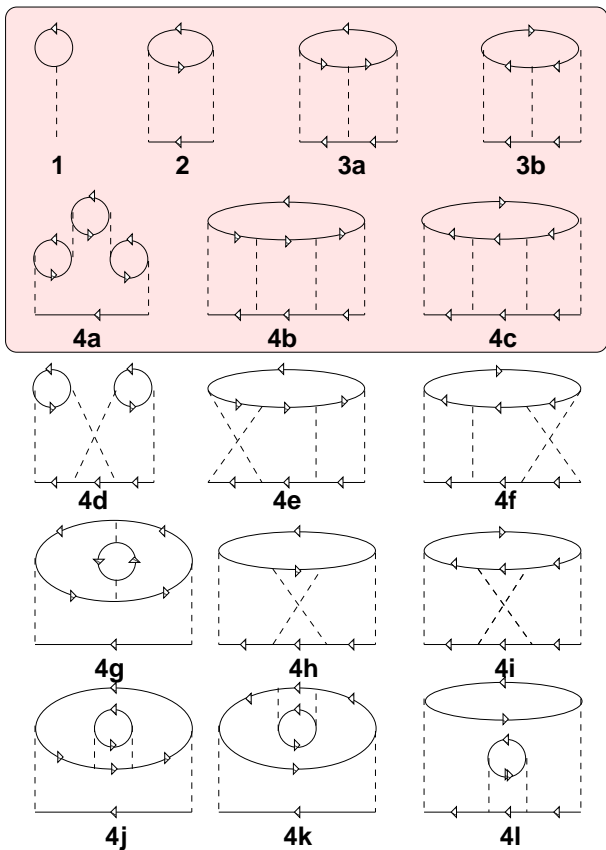
FIG. 1: Feynman diagrams for the Hubbard model to 4th order. Shaded diagrams are computed for a large cluster, while the remaining diagrams are computed for the smaller cluster. In our scheme, an infinite number of FLEX diagrams is considered, and the remaining diagrams are calculated using QMC, which is a non-perturbative method.
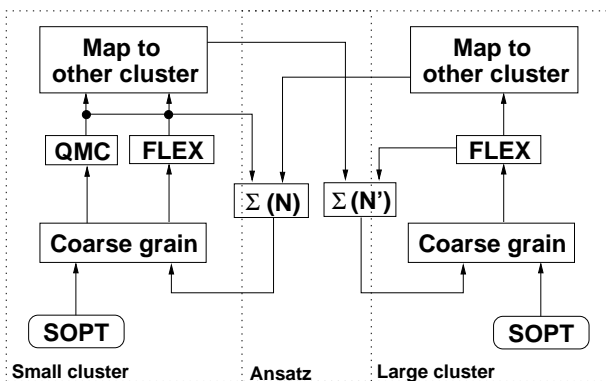


FIG. 2: Flow chart showing the self-consistent procedure for the ansatz. Iteration is initialized using second order perturbation theory (SOPT). The flow then continues with the calculations for both cluster sizes, which are carried out consecutively. Once convergence is reached, analysis is carried out on the results from the large cluster to compute quantities of interest, such as the local moment and the Fermi-surface.
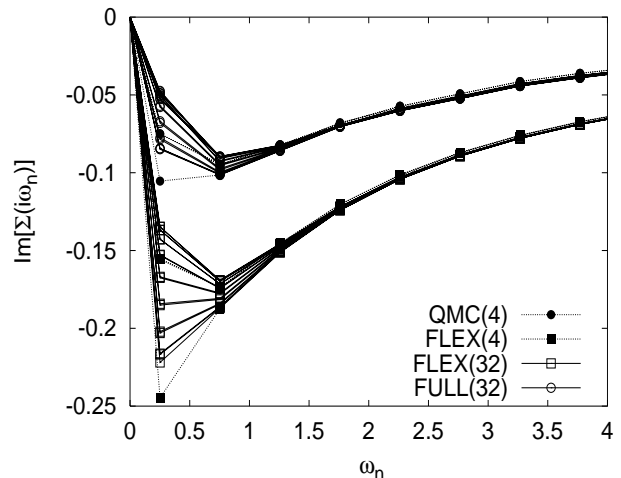


FIG. 3: Self-energy ansatz by contribution, including the QMC part for the small cluster (filled circles with solid lines), the FLEX part for the small cluster (filled squares with solid lines), the FLEX part for the large cluster (open squares with dashed lines),and the combination of these into the ansatz for the large cluster (open circles with dashed lines). $U = 0.8W$, $T = 0.08$, $N_C = 4$, $N_C' = 32$, $D = 1$, $n = 0.5$. For each of the self-energy contributions, there are a number of curves representing the different contributions at each momentum point as the Brillouin zone is crossed. Causality is preserved for this value of $U$. FLEX overestimates the self-energy, while QMC has the correct order of magnitude, but has insufficient details of the momentum dependence. The ansatz corrects the momentum dependence, while keeping the value of the self-energy at the appropriate order of magnitude.

Consequently, $-\omega_n \text{Im}\Sigma(\mathbf{k}, i\omega_n) > 0$ as a consequence of causality. We employ violations of this inequality as a sufficient but not necessary indication of the causality violation of our formalism.

In figure 3, we examine the self-energy in 1D for $N_C = 4$, $N_C' = 32$, $U = 0.8W$ and $T = 0.08$ at half-filling. All components of the ansatz are shown: The QMC self-energy for the smaller cluster (filled circles), the FLEX self-energy for the smaller cluster (filled squares) and the FLEX self-energy for the larger cluster (open squares). The result of the ansatz is also shown for the larger cluster only (open circles). The combination of 1D lattice and intermediate coupling results in an extreme test case for the ansatz, and causality can be seen to hold for both large and small clusters.

There are two ways in which causality may be violated. The first relates to the nature of the ansatz. In order to avoid overcounting of diagrams, FLEX diagrams on the small length scale are subtracted before new diagrams on a larger length scale are reinserted. Therefore, even when the FLEX method gives causal results, the ansatz may return a non-causal self energy. The FLEX parts of the ansatz are designed to return the correct momentum dependence to the self energy, and may be seen as a
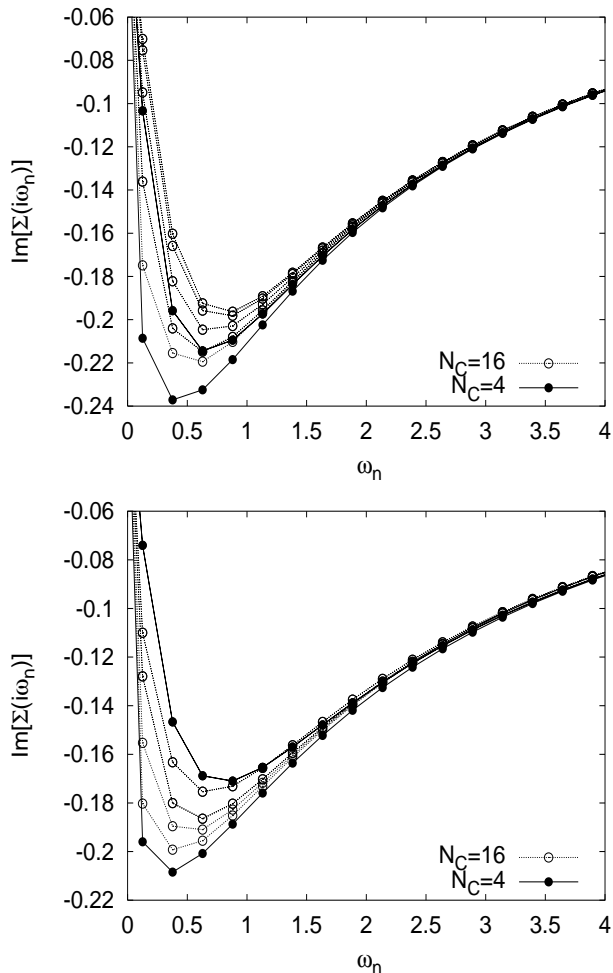
FIG. 4: Matsubara axis self energy calculated using FLEX. The top panel shows the self-energy for $U = W$, $D = 1$ and the bottom panel for $U = 0.5W$, $D = 2$. In both cases, the result from large and small clusters are sufficiently close to one another to avoid causality problems in the ansatz.

perturbation to the QMC segment of the self energy,

$$\Sigma(\mathbf{k}) = \Sigma_{\mathrm{QMC}} + \Delta\Sigma(\mathbf{k}) \qquad (7)$$

In order to avoid causality problems resulting from the subtraction of FLEX diagrams, small-length-scale clusters should be as large as possible, with a minimum requirement that $N_C > 1$. The reason for this is clear for very large QMC clusters, since in the limit that $N_C \to N'_C$, both FLEX solvers return the same results, and $\Delta\Sigma(\mathbf{k}) \to 0$ i.e. causality is guaranteed. For a good cancellation of the FLEX terms, the small and large cluster FLEX self-energies should both be on the large N scaling curve. We demonstrate the scaling behavior of the FLEX approximation in figure 4 (a pure FLEX calculation is used). The imaginary part of the self-energy from the FLEX approximation is shown. Both 1D and 2D calculations are carried out, and $N_C$ chosen to be representative of cluster sizes used in this paper. For the 2D case, the $N_C = 4$ self-energy doesn't sit directly on

the scaling curve. However, it has the correct form to promote causality since the extremal behavior is similar to that of the large cluster. In general, for smaller $U$, less cluster points are needed to fall on the scaling curve (with a minimum of $N_C = 4$ for both 1D and 2D systems). For larger $U > W$, the minimum $N_C$ required to see correct scaling behavior in the FLEX approximation is expected to increase. We suggest that the use of the ansatz should be limited to couplings that are no bigger than the bandwidth.

If the self-energy contributions from the FLEX approximation lie far away from the scaling curve, then the magnitude of $\Delta\Sigma(\mathbf{k})$ can be as large as the QMC part. FLEX inherently overestimates the magnitude of the self-energy, so errors are expected to be amplified at strong coupling. For this reason, use of the DMFT ($N_C = 1$) as a small cluster solver is not advised unless the temperature is high, or the coupling is weak.

Causality problems may also originate from the FLEX instability. FLEX is constructed from a geometric series, which imposes a condition on the susceptibilities: $\chi_{pp}(\mathbf{0}, 0), \chi_{ph}(\mathbf{Q}, 0) < 1$. At very high temperatures, both susceptibilities are small, and the geometric condition is met. As temperature decreases, the susceptibilities grow. In 1D and 2D, where the Mermin-Wagner theorem holds, the FLEX instability should only cause minor issues of numerical instability, since the susceptibilities are never expected to diverge (N.B. Some numerical effort is still required to avoid the instability). In 3D, however, FLEX predicts a phase transition at moderate temperatures. Below that transition, the unbroken symmetry approximation is neither causal nor valid. Lower temperatures could only be accessed by extending the approximation to include the anomalous Green functions associated with broken symmetry states. It is unlikely that the Stoner criterion $\chi_{ph} = 1$ is meaningful in the ansatz scheme, so there will be regions of the parameter space that cannot be reached in 3D. In order to investigate the 3D phase diagram with this scheme, it is essential that the FLEX instability occurs at lower temperatures than the true phase transition. Alternatively a large cluster solver such as 2nd order perturbation theory could to be applied. The phase transition would be measured through the divergence of the relevant 2-particle susceptibility. To calculate this quantity, it would be necessary to introduce an additional ansatz for the irreducible vertex function. This would be quite involved, and is left for a future publication.

Finally, we note that FLEX (as an extension of the T-matrix approximation) is exact for dilute systems, and the ansatz is therefore expected to be exact in the region of low doping. So long as reasonable temperatures are maintained, results should be applicable to a wide range of couplings and dopings. For dopings closer to half-filling, the results of testing show the approximation to be valid for couplings of up to the band width.
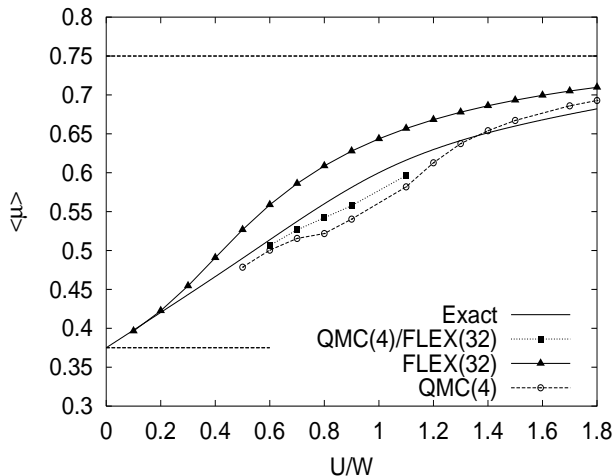
5



FIG. 5: Comparison of the local moment calculated using FLEX and the ansatz-based technique presented in this paper against the exact Bethe-ansatz result. All schemes have the same weak-coupling behavior. Although FLEX overestimates the moment at strong coupling, the solution from our ansatz shows promising results. Both the underestimation of the moment that results from small cluster simulations, and the overestimation inherent in the FLEX approximation are corrected.

## IV.  1D MODEL

In this section, the applicability of the hybrid FLEX/QMC approach to the 1D Hubbard model is discussed. Since the exact ground state of the 1D case is known from the Bethe ansatz solution [2], a quantitative comparison of certain quantities is possible.

While the FLEX approximation predicts the correct AFM transition temperature (the Mermin–Wagner theorem requires that there is only a transition at absolute zero), it is well known that FLEX describes local moment formation incorrectly for couplings of the order of the bandwidth. The fundamental definition of the local moment is,

$$< \mu >= S(S+1) < (n_\uparrow - n_\downarrow)^2 >= \frac{3}{4}(< n > -2 < D >)$$
(8)

where $< D >=< n_\uparrow n_\downarrow >$ is the expectation value of the double occupancy. [?] Since the potential energy term of the Hubbard model is $UD$, $< D >$ can be extracted from the expectation value of the potential energy via,

$$< V >= \text{Tr}[\Sigma(\mathbf{K}, i\omega_n)G(\mathbf{K}, i\omega_n)] = U < D >$$
(9)

Figure 5 shows the local moment versus coupling, calculated using several different techniques (FLEX, the ansatz-based FLEX/QMC technique presented in this paper, and the exact ground state solution). There is a difference in temperature between the exact Bethe-ansatz solution of Lieb and Wu ($T = 0$) [2] and the approximate solutions computed here ($T = 0.16W$) [?]. The temperature is still low enough to see the non-trivial effects of
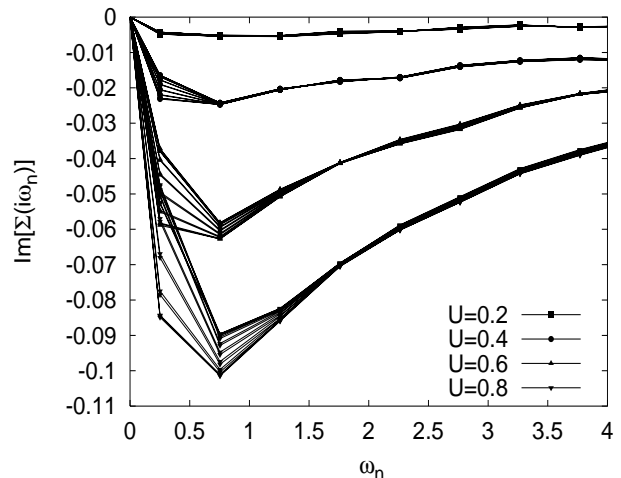


FIG. 6: Self energy in 1D for various couplings. $T = 0.08$, $N_C = 4$, $N'_C = 32$, $D = 1$, $n = 0.5$. Each set of curves represents the variation of the self-energy across the Brillouin zone. Note how the momentum dependence becomes more pronounced as coupling increases. No causality problems are found for couplings of similar size to the bandwidth.

spatial fluctuations. The hopping, $t = 0.25$, fixes the the bandwidth of the non-interacting problem to unity (therefore the interaction energy scale for the boundary between weak and strong coupling regimes is $U = 1$). Calculations are carried out for values of $U$ up to the bandwidth to examine behavior outside the perturbative regime. The exact result for a 1D problem calculated from the Bethe ansatz solution is shown, and compared with the 4 site QMC, the FLEX solution for a cluster size of $N_C = 32$, and the hybrid FLEX/QMC scheme.

The results in figure 5 shows that all schemes have the same weak coupling behavior. The gradient of the low $U$ curve increases with larger cluster size and decreased temperature to converge on the Bethe-ansatz solution. It can be seen that FLEX overestimates the moment at strong coupling, i.e. it underestimates the double occupancy. Alternatively, results from the 4 site QMC approximation are inclined to underestimate the local moment at intermediate coupling, probably because the mean-field nature of the $N_C = 4$ DCA used here predicts a metal insulator transition at a critical coupling $U = U_C$, rather than at $U = 0^+$ as expected in 1D. The solution from the new ansatz shows promising results. The moment has the same weak coupling behavior seen in all the presented approximations. More importantly, the overestimation of the moment that was predicted by the FLEX approximation has been corrected. Remarkably, the new hybrid method predicts a moment that closely follows the exact solution, and the mean-field like behavior of the DCA is greatly reduced.

The self energy predicted by the hybrid scheme is shown in figure 6. Calculations are also carried out for the 1D system for a series of couplings. In this case, the temperature is $T = 0.08W$. Groups of curves with sim-

ilar asymptotic behavior belong to the same coupling, and differ only by their location in the Brillouin zone. As coupling increases, the self-energy gets larger, as expected. As compared to a conventional QMC calculation with $N_C = 4$, the self-energy has significantly more detail, representing many more points in the Brillouin zone. This momentum dependence is most important for intermediate coupling results.

By examining the $U = 0.8W$ result, the advantage of the hybrid method over the traditional approach can be seen. With a QMC calculation, a linear interpolation would be used to extract the lattice self energy. This would mean that all the self-energy curves would be equidistant. In contract, the lines at the extremes (which correspond to the center and edge of the Brillouin zone) are clearly much closer together. In fact, for QMC cluster sizes up to $N_C = 6$ in 1D, only extremal behavior can be predicted, and therefore it is apparent that the Hybrid scheme generates results which are much closer to the true lattice self-energy.

## V. 2D MODEL

An important quantity that can shed light on the physics of correlated electron systems is the existence and shape of the Fermi-surface. The Fermi-surface may be used as input for a variety of other theoretical techniques, and may be also be compared directly with results from experimental methods such as angle-resolved photo-emission spectroscopy (ARPES) and de Haas van Alphen measurements. In this section, we examine features of the Fermi surface in 2D, by investigating the momentum-dependent electron density across the Brillouin zone. The form of this quantity is closely connected to the shape of the Fermi-surface.

The momentum dependent electron occupation may be calculated using the following formula,

$$n_{\mathbf{k}} = T \sum_n G(\mathbf{k}, i\omega_n) \exp(i\omega_n 0^+) \qquad (10)$$

where the lattice Green function has been constructed from the linear interpolation of the large cluster self-energy. The magnitude of the gradient of this quantity $|\nabla n_{\mathbf{k}}|$ is related to the Fermi-surface, since the gradient is largest at the Fermi-surface.

The calculations in this section are performed at $T = 0.04$ with coupling $U = 2.0 = W$. An $N_C = 4$ QMC cluster is used throughout. 48 time slices were used for the Trotter decomposition of the QMC cluster. The 2D model has a simple cubic tight-binding dispersion with $t_x = t_y = 0.25$ and a small interplane hopping $t_z = 0.005$ to stabilize the solution. The Fermi-surface has been computed using the hybrid scheme for a series of fillings and large cluster sizes.

One of the underlying aims of the hybrid scheme is to predict features consistent with very large systems, without the need for expensive QMC simulations. We
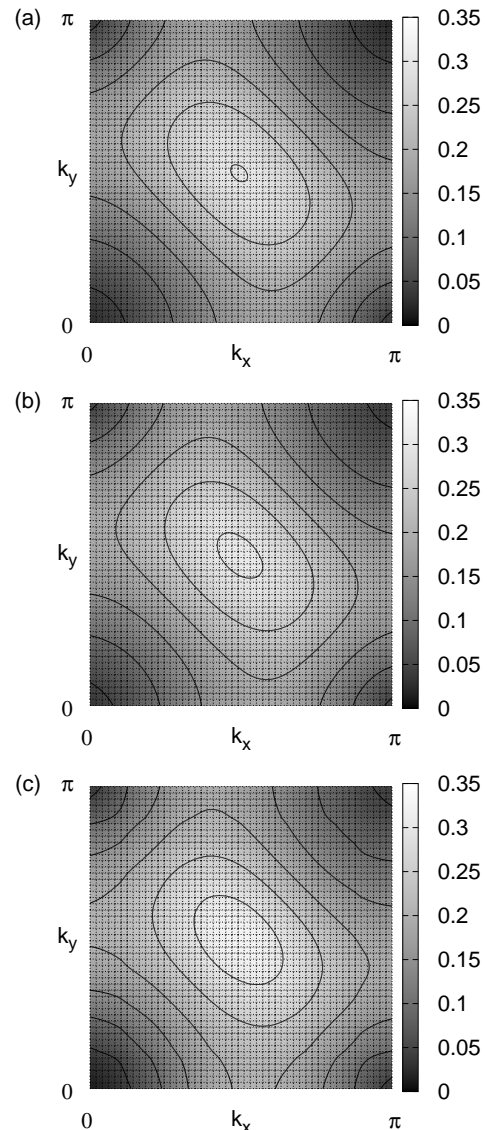


FIG. 7: Variation of the Fermi-surface, $|\nabla n(\mathbf{k})|$ with cluster size. Calculations are performed with $U = 2$, $T = 0.04$, $\mu = 0.075$ and (a) $N_C' = 4$, (b) $N_C' = 16$ and (c) $N_C' = 256$. Larger cluster sizes lead to a more well defined surface, with a more electron-like character (see c). Contours are spaced every $\Delta|\nabla n(\mathbf{k})| = 0.05$.

first investigate the variation in $|\nabla n_{\mathbf{k}}|$ as the cluster size is increased from $N_C' = 4$ to $N_C' = 256$, when the chemical potential is set to $\mu = 0.075$ corresponding to a 2D Hubbard model just away from half-filling. The results of these calculations are shown in figure 7. As cluster size is increased, $|\nabla n_{\mathbf{k}}|$ becomes sharper and better defined. Also a small number of finer features emerges. Although $N_C' = 64$ is not shown, we note that the $N_c' = 64$ cluster is
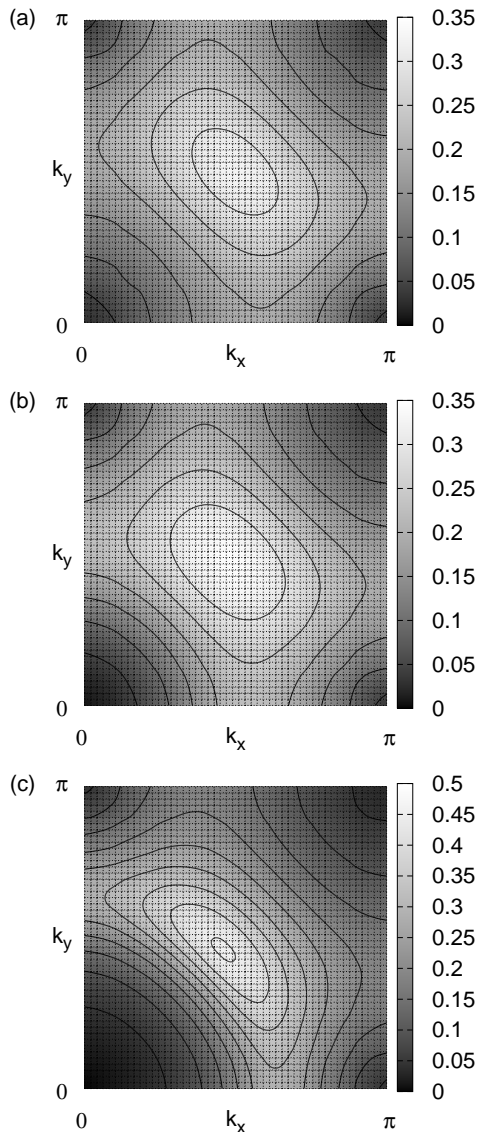
(a)

(b)

(c)

FIG. 8: Evolution of the Fermi-surface in 2D, $|\nabla n(\mathbf{k})|$, for various fillings calculated using the hybrid FLEX/QMC scheme. All calculations are performed with $U = 2 = W$, $T = 0.04$, $N_c = 4$ and $N'_C = 256$. Values of the chemical potential are (a) $\mu = 0.025$, (b) $\mu = 0.1$ and (c) $\mu = 0.25$. For values of filling close to half-filling, no Fermi-surface is seen, with a very diffuse gradient to the momentum dependent electron density. (b) shows an interim value, where the Fermi-surface begins to form as the edge of the gap is reached. It can be seen that the central peak develops greater intensity, and the beginnings of a curved Fermi-surface can be seen close to the $(\pi/2, \pi/2)$ point. Finally in (c) a clearly defined Fermi surface is seen, with significant additional intensity. Contours are spaced every $\Delta|\nabla n(\mathbf{k})| = 0.05$
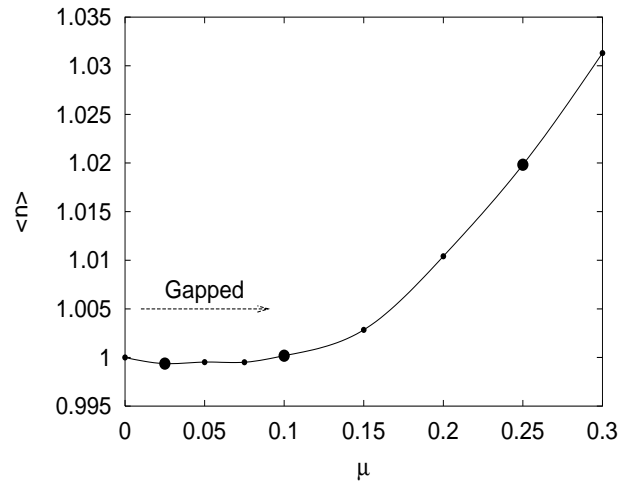


FIG. 9: Evolution of the filling, $< n >$, with chemical potential, $\mu$. The signature of a gapped state can be seen at low chemical potentials, with no variation of filling as chemical potential is increased. A gap of at least $0.05W$ can be seen ($W = 2$ in this case). The three larger points correspond to the chemical potentials chosen in figure 8. The line is a guide to the eye.

close to convergence, with only small differences between $N'_C = 64$ and $N'_C = 256$. The larger cluster seems significantly more electron- than hole-like, indicating that the band-gap inherent at half filling has become slightly narrower, although the diffuse nature of the surface indicates that the system is not in a Fermi-liquid state (this is to be expected close to half-filling, since there are significant spin-fluctuations).

An aspect of the 2D Hubbard model that is of general interest is the evolution of the Fermi-surface as filling is changed. In a dilute system, the Hubbard model is well described by the T-matrix approximation, which predicts Fermi-liquid behavior. At the other extreme, the half-filled system has a metal-insulator transition, with strong spin-fluctuations due to the proximity of a phase transition to the anti-ferromagnetic state at absolute zero. Also, non-Fermi-liquid pseudogapped behavior has been reported for the 2D Hubbard model a little off half filling.

In figure 8, $|\nabla n_{\mathbf{k}}|$ is shown for the $N_C = 4$, $N'_C = 256$ scheme. The results are computed for a fixed $U$ and temperature value, and only the filling is varied. Representative graphs are shown to demonstrate the gapped state, the movement between gapped and metallic states, and the beginnings of the Fermi-surface.

When close to half of the electronic states are occupied $< n >= 1.0$ (see the result for $\mu = 0.025$), $|\nabla n_{\mathbf{k}}|$ is quite disperse, with available electronic states across the Brillouin zone, and no clearly defined maximum associated with a Fermi-surface. As filling is increased to $< n >= 1.002$ ($\mu = 0.1$), the Fermi-surface becomes better defined, and some curvature due to free electrons is evident. For larger fillings, $< n >= 1.02$ ($\mu = 0.25$), the beginnings of an electronic Fermi-surface are evident. In

addition to the electron-like states, an unusual hole-like surface can be seen. This is smaller in magnitude than the maximum corresponding to the electronic states, but it persists into the metallic state.

In order to quantify the transition between gapped and metallic states, the expectation value of the occupation, $< n >$, has been calculated as a function of the chemical potential, $\mu$. The results are shown in figure 9. For chemical potentials of up to the order of $\mu = 0.1$, the filling does not vary, sitting at $< n > = 1.0$ or half-filling (there is a slight error due to the QMC algorithm). This indicates the presence of a gap which is approximately 5% of the band width. Once the metallic regime is reached, the filling doesn't vary very quickly, which suggests that there are very few states close to the Fermi-energy. This may be an indication of pseudogapped behavior.

## VI. CONCLUSIONS

We have introduced a new technique for the simulation of the Hubbard model. In this technique, short length-scale fluctuations are treated using QMC techniques, and the solution is supplemented with long length scale physics from the FLEX approximation.

We have demonstrated that the new technique is successful at simulating the Hubbard model in 1D and 2D, provided that the QMC cluster is sufficiently large. In particular, we find that results for the 1D Hubbard model at low temperatures are very close to the exact Bethe ansatz solution. The new hybrid method works well for couplings up to the order of the band-width. This is important, since spatial fluctuations on all length scales are expected to make a major contribution to the physics of the 1D model. It is therefore expected that the hybrid QMC/FLEX calculations will give important insight into the 1D problem, while remaining numerically cheap. In 2D, the ansatz has been applied to the calculation of the Fermi-surface. We demonstrate that very large clusters of $N_C' = 256$ can be simulated. For coupling of the order of the band-width, we demonstrate the evolution from insulating to metallic behavior.

The new technique is important from two view points. First, QMC simulation of large clusters is very expensive, with computing time growing quickly with cluster size. Therefore, any improvement on the convergence properties of the DCA method will aid in the accurate simulation of lattice models. Second, it has been proposed that a similar technique be used to combine DMFT with the *ab-initio* GW approximation [12]. In fact the two cluster solver approach is quite general, and it is expected that other models could be accurately treated using similar techniques.

## VII. ACKNOWLEDGEMENTS

[1] J.Hubbard, Proc. Royal Society **276**, 238 (1963).
[2] E.H.Lieb and F.Y.Wu, Phys. Rev. Lett. **20**, 1445 (1968).
[3] A.Georges, G.Kotliar, W.Krauth, and M.Rozenburg, Rev. Mod. Phys **68**, 13 (1996).
[4] M.Jarrell, Phys. Rev. Lett. **69**, 168 (1992).
[5] R.Bulla, T. Pruschke, and A.C.Hewson, Physica B **259-261**, 721 (1999).
[6] M.H.Hettler, A.N.Tahvildar-Zadeh, M.Jarrell, T. Pruschke, and H.R.Krishnamurthy, Phys. Rev. B **58**, R7475 (1998).
[7] M.Jarrell, Th.Maier, M.H.Hettler, and A.N.Tahvildarzadeh, Europhys. Lett. **56**, 563 (2001).
[8] N.E.Bickers and D.J.Scalapino, Ann. Phys. **193**, 206 (1989).
[9] K. Aryanpour, M. H. Hettler, and M. Jarrell, Phys. Rev. B **65**, 153102 (2002).

[10] M.Jarrell, Th.Maier, C.Huscroft, and S.Moukouri, Phys. Rev. B **64**, 195130 (2001).
[11] J.E.Hirsch and R.M.Fye, Phys. Rev. Lett. **56**, 2521 (1986).
[12] P.Sun and G.Kotliar, Phys. Rev. B **66**, 85120 (2002).
[13] The ansatz may be thought of as constructed from a generating functional $\phi = \phi_{QMC}^{N_C} - \phi_{FLEX}^{N_C} + \phi_{FLEX}^{N_C'}$. From this definition, the self-energy may be defined as the first functional derivative, and the irreducible vertices as the second functional derivative.
[14] Note that in some definitions of the local moment, the prefactor $S(S + 1)$ is omitted.
[15] The relatively high temperature used here avoids instabilities at lower temperatures